doi:10.1111/mmi.12361

The crystal structure of the cell division amidase AmiC reveals the fold of the AMIN domain, a new peptidoglycan binding domain

Mathieu Rocaboy,[1] Raphael Herman,[1] Eric Sauvage,[1] Han Remaut,[2] Kristof Moonens,[2] Mohammed Terrak,[1] Paulette Charlier[1] and Frederic Kerff[1]***

[1]*Centre d'Ingénierie des Protéines, University of Liège, Liège, Belgium.*

[2]*VIB Laboratory of Structural and Molecular Microbiology, VUB, Brussels, Belgium.*

Summary

Binary fission is the ultimate step of the prokaryotic cell cycle. In Gram-negative bacteria like *Escherichia coli*, this step implies the invagination of three biological layers (cytoplasmic membrane, peptidoglycan and outer membrane), biosynthesis of the new poles and eventually, daughter cells separation. The latter requires the coordinated action of the N-acetylmuramyl-L-alanine amidases AmiA/B/C and their LytM activators EnvC and NlpD to cleave the septal peptidoglycan. We present here the 2.5 Å crystal structure of AmiC which includes the first report of an AMIN domain structure, a β-sandwich of two symmetrical four-stranded β-sheets exposing highly conserved motifs on the two outer faces. We show that this N-terminal domain, involved in the localization of AmiC at the division site, is a new peptidoglycan-binding domain. The C-terminal catalytic domain shows an auto-inhibitory alpha helix obstructing the active site. AmiC lacking this helix exhibits by itself an activity comparable to that of the wild type AmiC activated by NlpD. We also demonstrate the interaction between AmiC and NlpD by microscale thermophoresis and confirm the importance of the active site blocking alpha helix in the regulation of the amidase activity.

Accepted 5 August, 2013. For correspondence. *E-mail fkerff@ulg.ac.be; Tel. (+32) 4366 36 20; Fax (+32) 4366 49 54; **E-mail paulette.charlier@ulg.ac.be; Tel. (+32) 4366 36 19; Fax (+32) 4366 49 54.

Introduction

In *Escherichia coli*, cytokinesis involves the synthesis of new peptidoglycan material at midcell, which after maturation evolves to become the new poles of the daughter cells. Septal peptidoglycan synthesis is directed by a complex of essential and accessory proteins called the divisome and composed of cytoskeletal proteins, peptidoglycan synthases and peptidoglycan hydrolases with their cognate regulatory proteins. This division machinery includes at least 17 proteins: FtsZ, FtsA, ZipA, ZapA, ZapB and ZapC, FtsE, FtsX, FtsK, FtsQ, FtsL, FtsB, FtsW, FtsI(PBP3), PBP1B, FtsN, and AmiC (den Blaauwen *et al.*, 2008). Division is initiated by the polymerization of FtsZ into a ring at midcell underneath the cytoplasmic membrane and the association with the FtsA, ZipA, ZapA, ZapB, ZapC and ZapD proteins (Bi and Lutkenhaus, 1991; Hale and de Boer, 1997; Durand-Heredia *et al.*, 2011; 2012; Galli and Gerdes, 2012). The downstream components are then sequentially recruited, either as single molecules or as preformed subgroups (e.g. FtsQ-FtsB-FtsL and FtsW-PBP3) (Buddelmeijer and Beckwith, 2004; Goehring *et al.*, 2006; Fraipont *et al.*, 2011). PBP3 is a specific DD-transpeptidase essential for septal peptidoglycan synthesis during cell division (Spratt, 1975; Botta and Park, 1981; Weiss and Hilgenfeld, 1997). Its function is believed to be coordinated with that of the major bifunctional glycosyltransferase – transpeptidase peptidoglycan synthase PBP1b during cell division (Bertsche *et al.*, 2006). The function of PBP1b is controlled by the inner membrane and essential divisome protein FtsN, which has been shown to interact and stimulate the activity of PBP1b *in vitro* (Müller *et al.*, 2007) and by the outer membrane linked lipoprotein LpoB, which has also been found to interact with and stimulate the activity of PBP1b (Paradis-Bleau *et al.*, 2010; Typas *et al.*, 2010).

The resulting septal PG formed by the divisome is shared between two daughter cells and must be split to allow cell separation. This process depends on the periplasmic peptidoglycan amidases AmiA, AmiB and AmiC (amidase_3 family, PF01520) (Heidrich *et al.*, 2001). These proteins are Zn^{++}-metallo-enzymes which hydrolyse the amide bond between the stem peptide L-Ala and the

N-acetylmuramic acid (MurNAc). Inactivation of the *amiA*, *amiB* and *amiC* genes results in the formation of long chains of cells, a phenotype that is also observed to a different extent in *amiA* and *amiC* single mutants but not in the *amiB* single mutant (Heidrich *et al*., 2001). AmiB and AmiC specifically localize to the division site, unlike AmiA, which shows dispersed localization in dividing cells (Bernhardt and de Boer, 2003; Peters *et al*., 2011). The localization of AmiC to the septal ring is mediated by the non-catalytic N-terminal AMIN domain and requires FtsN (Bernhardt and de Boer, 2003). The activities of the three periplasmic N-acetylmuramyl-L-alanine amidases are regulated by two LytM domain containing proteins (NlpD and EnvC), which do not seem to possess any enzymatic activity (Uehara *et al*., 2009; Peters *et al*., 2013). Other LytM proteins with PG hydrolase activity have been identified in some Gram-negative as well as Gram-positive species such as *Staphylococcus aureus* (Collier, 2010; Möll *et al*., 2010; Poggio *et al*., 2010; Sycuro *et al*., 2010). EnvC specifically activates AmiA and AmiB and NlpD specifically activates AmiC (Uehara *et al*., 2010). Both EnvC and NlpD activators also localize to the division site (Bernhardt and de Boer, 2003; Uehara *et al*., 2009). Unlike EnvC, AmiB and NlpD require FtsN for localization. A complex regulation mechanism involving proteins localization, peptidoglycan synthesis and degradation, and probably specific septal PG architecture is taking place during cell division (Peters *et al*., 2011). The *E. coli* mutant lacking EnvC and NlpD forms long cell chains that resemble the triple amidases mutant, which confirms their essential roles in cell separation (Uehara *et al*., 2009). The amidase activation by EnvC has been found to be regulated by the ATP-binding cassette (ABC) transporter-like complex FtsEX (Yang *et al*., 2011). This shows that cell wall hydrolysis at the division site leading to cell separation is tightly regulated to prevent uncontrolled cell lysis. Further, the interaction of FtsE with FtsZ suggests a coordination between the hydrolase activity during cell division and Z-ring driven constriction (Corbin *et al*., 2007).

Five structures of proteins belonging to the amidase_3 family have so far been solved. The activities of four of them appear to be unregulated: the bacteriophage PSA endolysin (Korndörfer *et al*., 2006), the catalytic domain of the CwlV amidase from *Bacillus polymyxa* (PDB code 1JWQ), a putative amidase from *Neisseria meningitidis* (PDB code 3NCZ) and the catalytic domain of the CD27L endolysin targeting *Clostridium difficile* (Mayer *et al*., 2011). The fifth structure is the catalytic domain of AmiB from *Bartonella henselae*. This amidase is characterized by the presence of an additional auto-inhibitory helix in the active site. The LytM domain responsible for the regulation of this protein thus needs to displace this helix for the enzyme to be fully active (Yang *et al*., 2011).

Table 1. Crystallographic data and model refinement statistics.

Diffraction data statistics	
Space group	$P2_12_12_1$
a, b, c (Å)	59.03, 68.44, 90.58
Resolution range (Å)	49.6–2.5 (2.56–2.5)
Unique reflections	13 337 (1907)
Completeness (%)	99.9 (99.8)
Redundancy	12.7 (7.3)
R_{merge} (%)[a]	20.1 (100.5)
R_{pim} (%)[b]	5.7 (39.7)
Average I/σ	12.8 (2.2)
Refinement statistics	
Resolution range (Å)	90.58–2.5 (2.56–2.5)
R_{cryst} (%)[c]	17.6 (24.2)
R_{free} (%)[d]	23.1 (31.4)
RMS deviations	
Bond lenghts (Å)	0.016
Bond angles (°)	1.625
Ramachandran analysis	
Favoured region (%)	95.9
Allowed region (%)	4.1
Outlier region (%)	0

a. $R_{merge} = \Sigma|Ii - Im|/\Sigma Ii$, where Ii is the intensity of the measured reflection and Im is the mean intensity of all symmetry related reflections.
b. R_{pim} denotes the precision-indicating merging R factor (Weiss and Hilgenfeld, 1997).
c. $R_{work} = \Sigma||F_o| - |F_c||/\Sigma|F_c|$, where F_o denotes the observed structure factor amplitude, and F_c denotes the structure factor amplitude calculated from the model.
d. R_{free} is similar to R_{work} but calculated with randomly chosen reflections that are omitted from the refinement.

In this work, we present the crystal structure of the N-acetylmuramyl-L-alanine amidase AmiC at a 2.5 Å resolution, revealing the fold of the N-terminal AMIN domain, which consists of two perfectly superimposable four-stranded anti-parallel β-sheets with conserved outer faces. We present evidences that this domain interacts with the peptidoglycan. In the C-terminal catalytic domain, a member of the amidase_3 family, an alpha helix obstructs the active site. We demonstrate the role of this helix in the control of the AmiC activity and also show a direct interaction between AmiC and its activator NlpD. We confirm that the mechanism of activation of AmiC by NlpD consists in the displacement of the alpha helix that blocks the access to the AmiC active site.

Results

Structure of AmiC

Overall fold. The 2.5 Å resolution structure of AmiC was solved by molecular replacement for the catalytic domain and model building for the AMIN domain (see *Experimental procedures* for details). The R_{cryst} and R_{free} values after refinement are 17.6% and 23.1% respectively (Table 1). The final electron density map shows a clear density for the whole protein except for five disordered segments

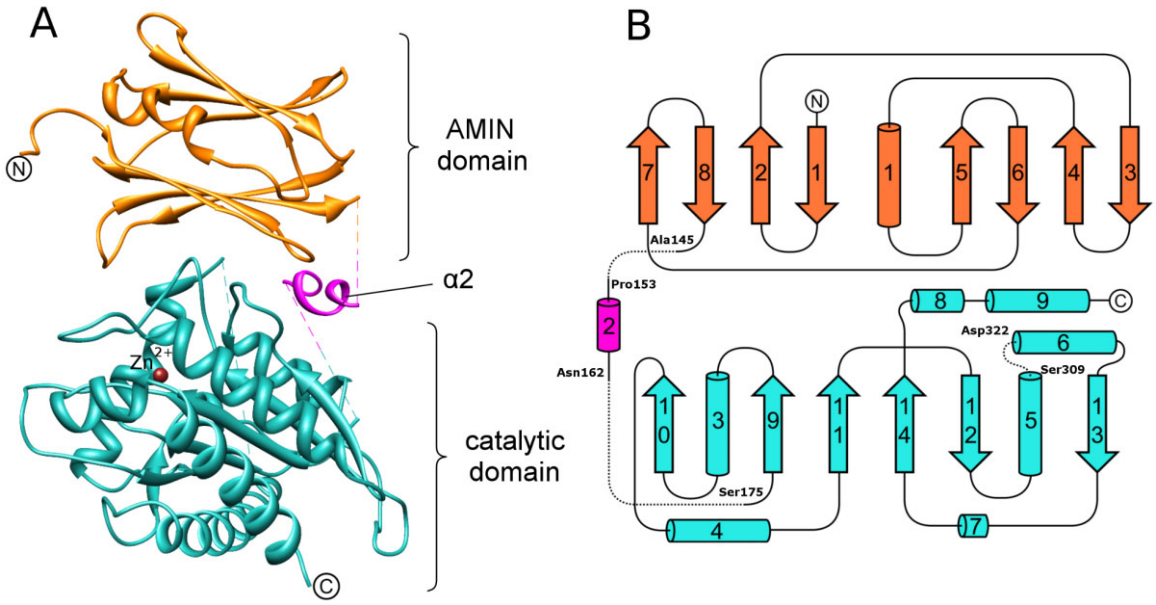

Fig. 1. Crystal structure of AmiC.
A. The AMIN domain, the linker and the catalytic domain are respectively shown in orange, violet and cyan.
B. Topology of AmiC. Stretches of missing residues are represented as dashed lines. Residues preceding and following the missing segments are labelled.

consisting of the first fifteen residues of the N-terminal purification tag, Asn146-Asp152, Lys163-Gln174, Lys310-Phe321 and the last nine residues at the C-terminus. AmiC is made of two structurally distinct domains linked by a flexible segment (Asn146-Gln160) containing the poorly defined α2 helix (Fig. 1). The N-terminal AMIN domain adopts an α-crystallin-like fold with two four-stranded anti-parallel β-sheets for which no structure has been reported so far. The C-terminal zinc-dependent catalytic domain (Ser175-Ala408) has an α/β fold with a six-stranded β-sheet flanked by α helices, and belongs to the amidase_3 family (Fig. 1) (Korndörfer *et al.*, 2006).

AMIN domain (Phe30-Ala145). One of the two β-sheets (β-sheet1) of the AMIN domain of AmiC is composed of strands β1-2-8-7 and the second one (β-sheet2) of strands β5-6-4-3 (Fig. 2B). An additional short α-helix (α1) located near the β1 and β5 strands closes one side of the β-sandwich. Four RxxxD/E motifs are present on strands β2 (Arg49xxxGlu53), β4 (Arg70xxxAsp74), β6 (Arg112xxxGlu116) and β8 (R137xxx-D141). These residues lie on the external face of the two central strands of each β-sheet (Fig. S1). Arg49 and Arg112 are involved in salt bridges with the aspartate of the two motifs located on the adjacent antiparallel strands (Asp141 and Asp74 respectively). This organization suggests that the repetition of the RxxxD/E motifs originates from the double duplication of a two-stranded ancestor encompassing one RxxxD/E motif on the second strand to form the AMIN domain (de Souza *et al.*, 2008). Both interactions Arg49/Asp141 and Arg112/Asp74 could be important to stabilize a folding intermediate or the final scaffold of the domain.

A ConSurf analysis with AmiC related proteins (Ashkenazy *et al.*, 2010) reveals a patch of conserved residues on the outer face of both β-sheets (Fig. 2D). Moreover, the superposition of β-sheet1 and β-sheet2 (Fig. 2A and C) reveals a striking similarity between them [root mean square deviation (RMSD) of 0.64 Å on 25 residues]. On each face, two small residues are surrounded by five charged residues and two hydrophobic ones (Fig. 2C). ConSurf scores range from 9.8 to 9.9 for each of these residues except for Phe63 and Leu65 with scores of 7.6 and 8.7 respectively. These residues are strictly conserved between β-sheet1 and β-sheet2 except for the Thr51 that is replaced by the shape-equivalent Val114 in β-sheet2.

β-Sheet1 shares numerous interactions with the catalytic domain. In particular, Glu199 of the catalytic domain seems to play the role of electrostatic anchor by sharing multiple hydrogen bonds with the AMIN domain via amino acids that form a hydrophilic pocket (Arg40, Trp42, Thr51 and Arg137). Moreover, Arg49 which belongs to the RxxxE motif of strand β2 interacts with the main chain carbonyl of Gly307 in the catalytic domain (Fig. S2). The AMIN domain also interacts with the C-terminus of helix α5 of the catalytic domain via hydrophobic interactions between Val131/Ala132/Phe134 and Leu304/Ile305 respectively. However, a PISA analysis (Krissinel and Henrick, 2007) of the inter-

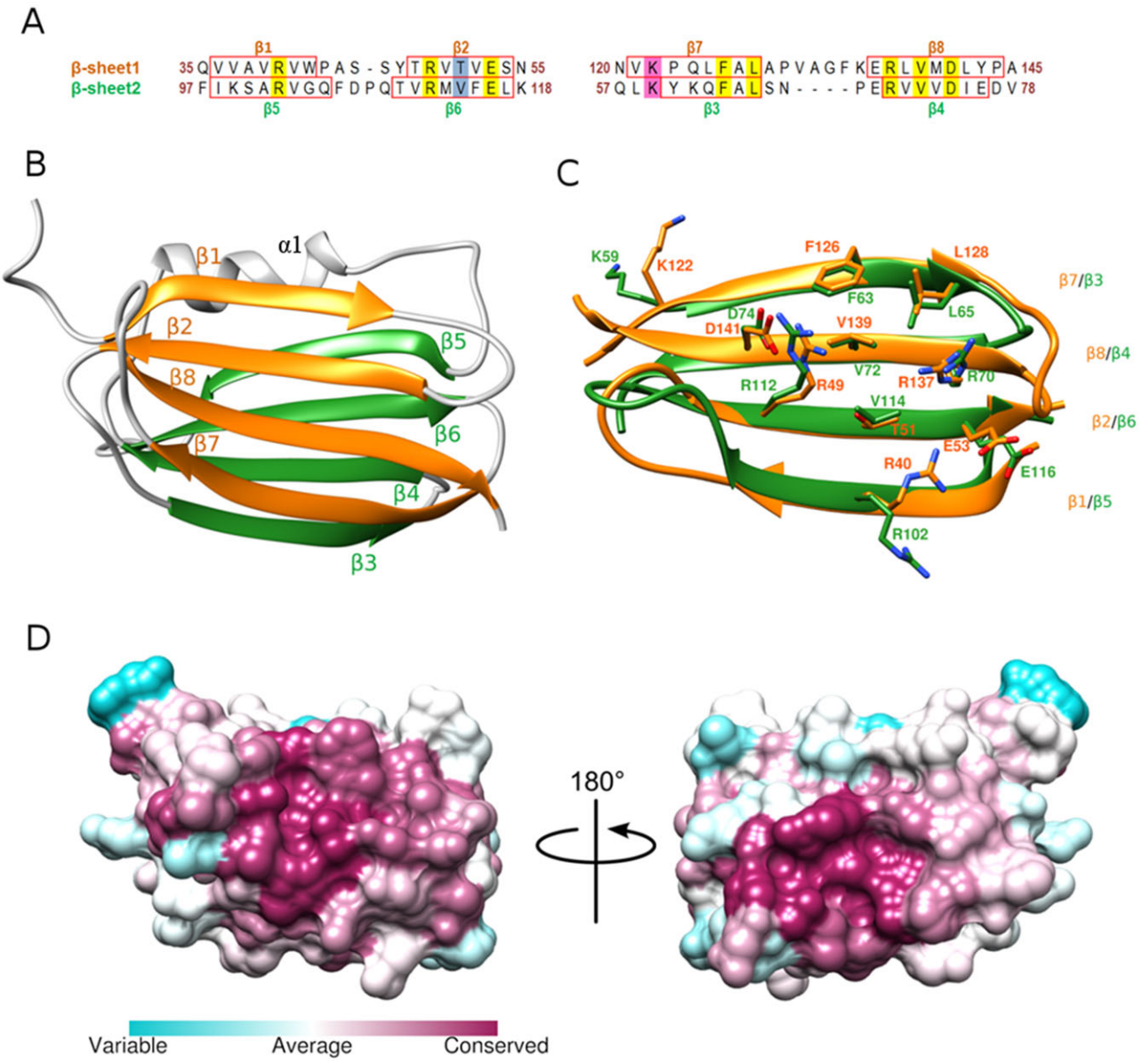

Fig. 2. AMIN domain of AmiC.
A. Sequence alignment of the two β-sheets composing the AMIN domain. β-strands are represented by red boxes. Surface residues conserved in the AMIN domains of amidases are highlighted: in yellow, for residues identical in β-sheet1 and β-sheet2 and in blue for residues of similar shape. Residues not conserved in AMIN domains but identical in the two β-sheets are represented in pink.
B. Cartoon representation of the AMIN domain. The β-sheet1 (strands β1-2-8-7) and the β-sheet2 (strands β3-4-6-5) are depicted in orange and green respectively. Coils and helix α1 are shown in grey.
C. Superposition of the two β-sheets of the AMIN domain. The colour code is the same as in Fig. 2B. Amino-acids highlighted in Fig. 2A are represented as sticks (nitrogens and oxygens are shown in blue and red respectively).
D. Surface representation of the AMIN domain. Conservation of amino-acids of AmiC related proteins is mapped onto the surface from poorly conserved in blue to highly conserved in purple.

action surface between the AMIN and catalytic domains provides a Complex Significance Score of 0 and thus may indicate a crystal packing artefact rather than a specific binding. This suggests a relative flexibility of the AMIN domain that could expose both its conserved surfaces for a simultaneous interaction with two similar partners.

Catalytic domain (Ser175-Ala408). The catalytic domain of AmiC consists in a strongly twisted six-stranded β sheet flanked by six α-helices (Fig. 1). The overall fold is conserved when compared with the five solved structures of the amidase_3 family (Korndörfer *et al.*, 2006; Mayer *et al.*, 2011; Yang *et al.*, 2011). RMSDs between alpha carbons

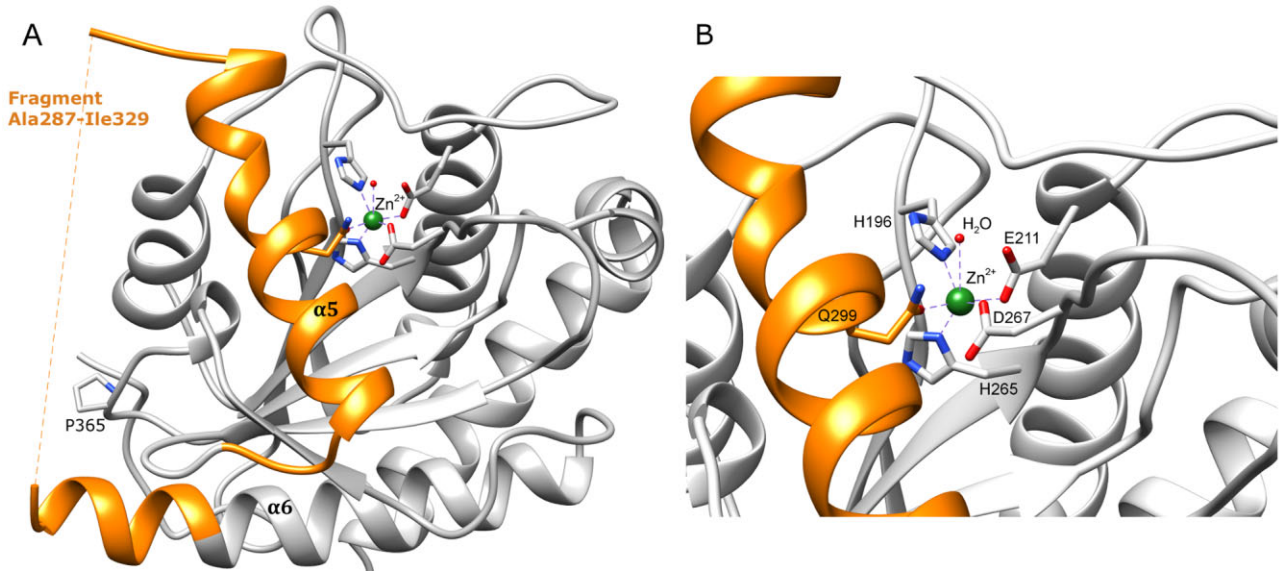

Fig. 3. Catalytic domain of AmiC.
A. Cartoon representation of the catalytic domain. The fragment removed to produce the mutant AmiCΔH5 (see in text) is depicted in orange. The catalytic zinc is shown in green.
B. Close-up on the catalytic site of AmiC. The catalytic zinc and the obstructing helix α5 are shown in green and orange respectively. The chelating residues are represented as sticks (nitrogens and oxygens are shown in blue and red respectively).

range from 0.8 Å (138 alpha carbons) with the N-acetylmuramyl-L-alanine amidase from *Bacillus polymyxa* (PDBID: 1JWQ) to 1.13 Å (85 alpha carbons) with the putative N-acetylmuramyl-L-alanine amidase from *Neisseria meningitidis* (PDBID: 3CZX). In the amidase_3 family, four residues involved in the catalytic activity are strictly conserved. Two histidines (His196 and His265) and one glutamate (Glu211) chelate the catalytic zinc ion (Fig. 3A and B). The fourth conserved residue (Glu373) is thought to be involved in the proton transfer during the catalysis in metallo-proteases (Christianson *et al*., 1989). As observed in the amidase orthologue AmiB from *B. henselae* [PDBID: 3NE8 (Yang *et al*., 2012)], the 43 amino-acid segment running from Ala287 to Ile329 contains the helix α5 (Thr290-Gly306) that obstructs the active site, and an extension to the helix α6 (Fig. 3A). Compared with the amidase_3 members with accessible active sites (PDB IDs: 1XOV, 3CZX and 1JWQ), this insertion induces slight conformational rearrangements in the loop connecting the strands β11 and β12. The most striking one is the position of Asp267 which is flipped in the direction of the catalytic site and coordinates the zinc ion (Fig. 3B) whereas in the other amidase_3 members, this aspartate is replaced by an asparagine oriented to the solvent. This conformation would be unfavourable in AmiC because of a steric hindrance with Leu295 present on helix α5. Zinc chelation by Asp267 could thus simply result from the blocking of the active site by helix α5 and this residue would not be involved in catalysis. Helix α5 also contains a glutamine residue (Gln299) which chelates the zinc ion. Asn300 and Asp303 are highly conserved in the amidase_3 members exhibiting the additional segment. Asn300 is in close contact with the loop connecting strands β13 and β14, while Asp303 interacts with the main chain nitrogen of Leu246 located at the beginning of helix α4 (Fig. S3). Asn300, Asp303 as well as Ser302, which is not a conserved residue, appear to be important for the stabilization of the helix in the active site and the interactions that they share with the rest of the catalytic domain have to be disrupted during the activation process. Moreover, the displacement of the obstructing helix requires a relative flexibility of the whole additional segment. This is supported by the absence of interpretable density for the Lys310-Phe321 segment connecting the helices α5 and α6. The corresponding segment (Glu303-Thr308) is also missing in the crystal structure of AmiB from *B. henselae*.

Sequence conservation analysis highlights a proline in position 365 (Fig. 3A) surrounded by polar residues (Gln254, Asp322, Lys363 and Asp366). This highly conserved patch (ConSurf scores ranging from 9.8 to 9.9) is located at the beginning of helix α6, close to the flexible loop connected to the obstructing helix α5 and thus constitutes a potential interaction surface with the activator NlpD. Such an interaction could induce slight conformational changes, like the disruption of the hydrogen bonds shared by Asn300 (see above), and release the obstructing helix from the active site.

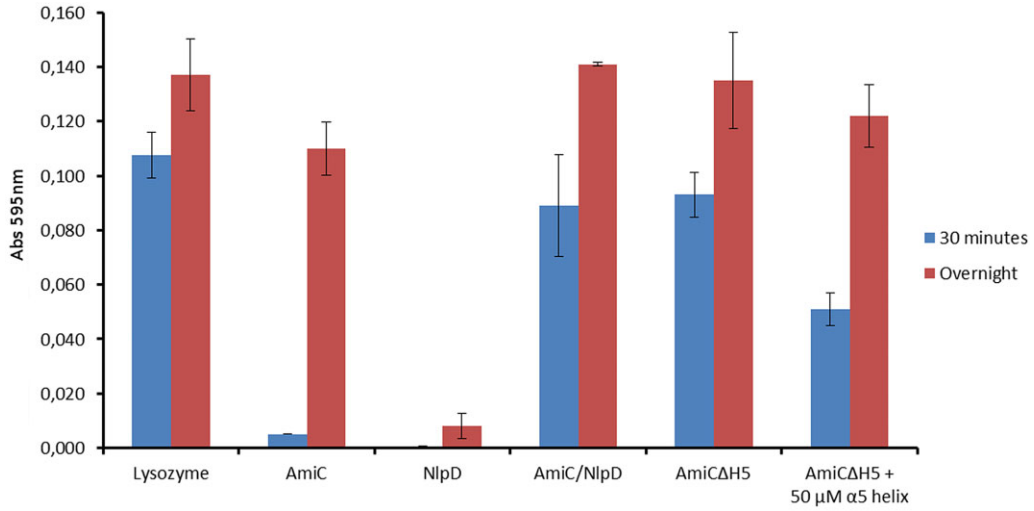

Fig. 4. Helix α5 of AmiC is involved in the activation mechanism by NlpD. The dye-release assay allows the following of the hydrolysis of RBB-labelled peptidoglycan. Each protein was used at 4 µM during 30 min (blue bars) or overnight (red bars). Lysozyme was used as positive control. AmiCΔH5 is the AmiC mutant lacking the Ala287-Ile329 segment. The α-helix is the peptide mimicking the Thr288-Gly306 segment of AmiC. Error bars represent standard deviations from three independent measurements.

AmiCΔH5 variant has maximal activity independent from NlpD

In order to characterize the activation mechanism of AmiC by the LytM factor NlpD, activity tests based on dye-release assay on Remazol Brilliant Blue (RBB)-labelled peptidoglycan were conducted (Fig. 4). Both proteins were purified and used at a 4 µM concentration and incubation times ranging from 30 min to nearly 15 h. The activation of AmiC by NlpD (Uehara *et al.*, 2010) was confirmed, as was the weak activity of AmiC for the shortest incubation time. NlpD did not show any significant activity by itself even for longer incubation times (overnight). Based on the structural data, we also produced and purified an AmiC mutant lacking the Ala287-Ile329 segment that includes helix α5 (AmiCΔH5). This construct was designed on the basis of the available structures of amidase_3 members lacking this additional segment in order to maintain the overall fold of AmiC. The level of activity of AmiCΔH5 against the RBB-labelled peptidoglycan is equivalent to that of AmiC activated by NlpD. Moreover, by adding a peptide mimicking helix α5 (Thr288-Gly306) at 50 µM, the measured activity of AmiCΔH5 was almost decreased by a factor 2. These results demonstrate that in the absence of helix α5, the AmiCΔH5 variant becomes unregulated and exhibits maximal activity without activation by NlpD. *In vivo*, such uncontrolled hydrolase activity would have severe consequences for the integrity of the bacterium leading to cell lysis.

AmiC directly interacts with NlpD

In vitro activation of AmiC by NlpD strongly suggests a direct interaction between these two cell division components. We tested the interaction by microscale thermophoresis, an immobilization-free technique that allows the monitoring of the displacement of molecules in a temperature gradient generated by an infrared laser. The behaviour of a particle in this gradient rests upon its mass, charge and solvation shell (Jerabek-Willemsen *et al.*, 2011). These properties are then altered when a binding partner is added to the system and titration series allow the determination of the binding affinity. Each protein was titrated against its potential partner and lysozyme was used as a negative control. In different experiments, each partner was labelled in turn with Dylight 650. Binding is detected for each titration involving the couple AmiC/NlpD and no binding is observed with lysozyme (Fig. 5). The apparent Kd values are 11.3 ± 1.5 µM with labelled NlpD and 15.5 ± 7.2 µM with labelled AmiC.

The AMIN domain of AmiC interacts with the peptidoglycan

The AMIN domain of AmiC is known to be necessary and sufficient for its proper localization to the division site (Bernhardt and de Boer, 2003). However, no binding partners have been identified so far. The interaction between the untagged AMIN domain of AmiC and the peptidoglycan was tested by pull-down experiments (Fig. 6). After two washing steps, a significant amount of the AMIN domain is released from the pelleted peptidoglycan in comparison with the control experiment without peptidoglycan. This assay clearly shows an interaction between the AMIN domain of AmiC and the peptidoglycan.

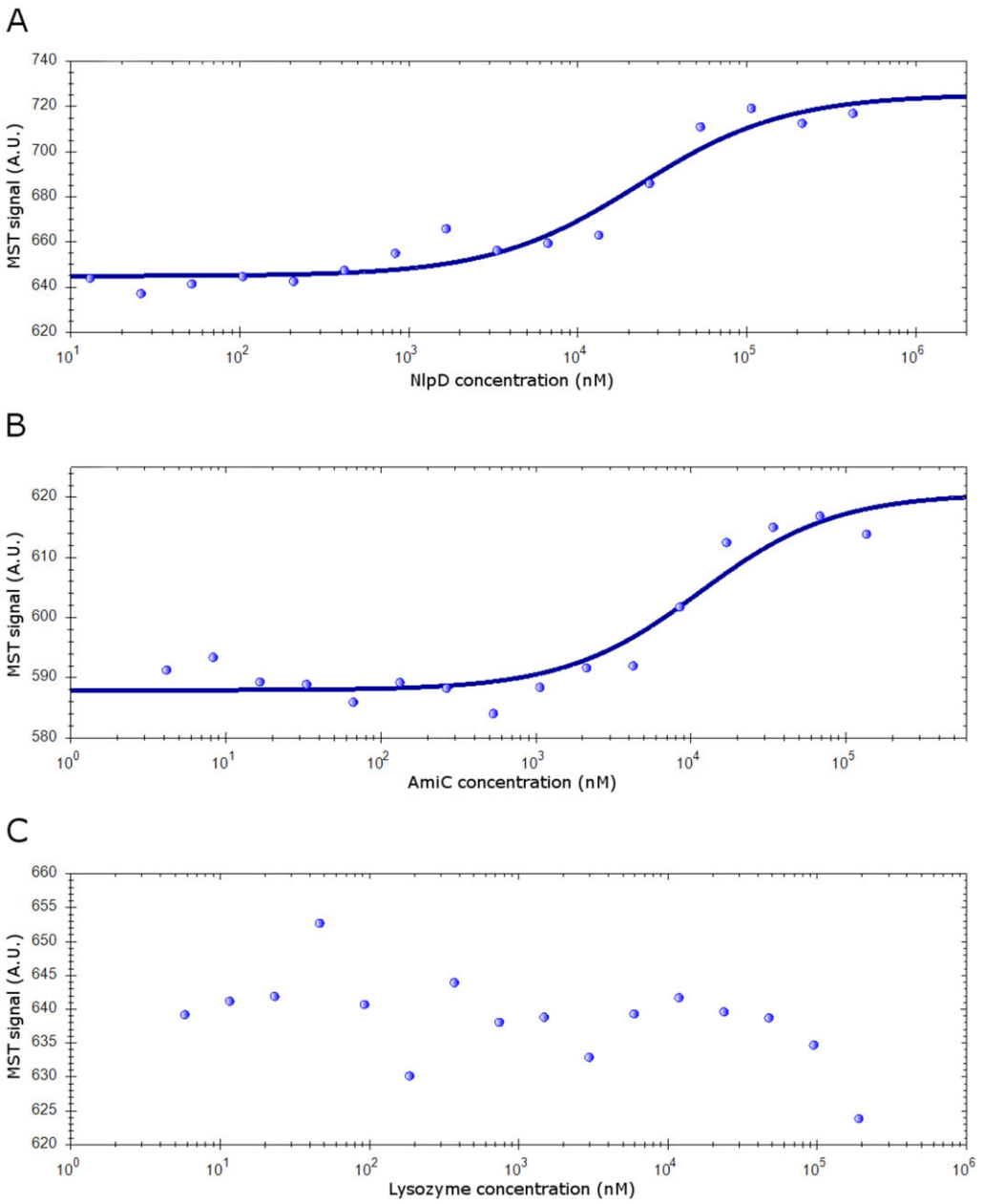

Fig. 5. AmiC directly interacts with NlpD. Microscale thermophoresis (MST) assays were realized with either AmiC labelled (A and C) or NlpD labelled (B) with Dylight 650. The negative control with lysozyme as binding partner did not exhibit the typical binding curve (C). Measures are represented by blue dots and fitted curves by blue lines.

Discussion

The final step of cellular division in *E. coli* consists in the splitting of one constricted cell into two daughter cells. This step requires the concerted action of three different N-acetylmuramyl-L-alanine amidases (AmiA/B/C) in order to cleave the septal peptidoglycan and release two independent cells. These enzymes have been recently shown to be regulated by LytM factors: EnvC activates AmiA/AmiB and NlpD activates AmiC (Uehara *et al.*, 2010).

The crystal structure of AmiC described in this paper highlights two structurally independent domains: the N-terminal AMIN domain and the C-terminal catalytic domain. The structure of the C-terminal amidase_3 domain clearly shows the obstruction of the active site by an α-helix confirming the observation made with the septal amidase AmiB from *B. henselae* (Yang *et al.*, 2012). This α-helix shares several contacts with the rest of the protein including a glutamine that chelates the catalytic zinc ion. The helix has to be displaced in order to accommodate the

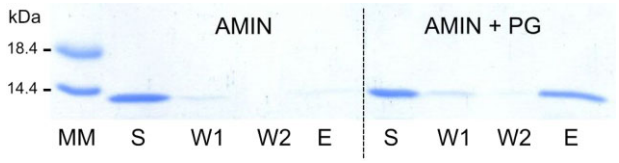

Fig. 6. The AMIN domain of AmiC interacts with the peptidoglycan (PG). 10 μg of the purified AMIN domain were incubated with peptidoglycan for 2 h at 4°C in the binding buffer. The supernatant (S) was collected after centrifugation at 14 000 *g* during 20 min. The supernatants of two washes followed by centrifugation (W1 and W2) and the remaining pellet resuspended with 2% SDS (E) were analysed by SDS-PAGE. Molecular markers are present in the first lane (MM).

peptidoglycan. For AmiC, this conformational change has been shown to be induced by the LytM factor NlpD (Uehara *et al*., 2010). Our thermophoresis experiments provide evidence that a direct interaction occurs between AmiC and its cognate activator NlpD. NlpD could directly compete with the AmiC active site for binding the inhibitory α-helix or recognize an adjacent area, inducing a conformation of AmiC that would prevent the α-helix from obstructing the active site. For the latter, a potential candidate is the conserved region of AmiC surrounding Pro365, which is relatively close to the catalytic site.

The addition of the synthetic form of the α5 helix partially restores the inhibited form of the enzyme. *In vitro* AmiC exhibits a basal activity suggesting a competition between the auto-inhibitory helix and peptidoglycan, with a clear preference for the closed state. In the presence of NlpD, the equilibrium is displaced towards the open state and the active site becomes freely accessible to peptidoglycan.

Although the AMIN domain is packed onto the C-terminal domain in the crystal structure, the presence of a 30 amino acids linker suggests a high flexibility between these two domains. The PISA analysis and the high homology between the AMIN exposed surface and the AMIN surface in contact with the catalytic domain also argue in favour of a crystallographic artefact for the interaction between these two domains. Interestingly, in the outer membrane associated lipoprotein NlpD, a long linker also connects the LysM domain, which binds to the peptidoglycan, to the LytM domain, which activates AmiC. Therefore, the length of these two linkers could spatially regulate the interaction between the activator domain of NlpD and the catalytic domain of AmiC for a correct cell separation process.

In the N-terminal AMIN domain, conserved residues on both outer faces suggest two symmetric interaction regions. The two RxxxD/E motifs present on each face of the AMIN domain represent almost half of the conserved residues. Their conservation and the striking symmetry of this domain suggest the recognition of a repeated pattern like the building blocks of peptidoglycan or the simultaneous binding to two identical divisome components. We have tested two potential binding partners of the AMIN domain: FtsN because of its importance for the recruitment of AmiC at the division site, and the peptidoglycan. Our attempts to find an interaction between purified FtsN and the AMIN domain by different pull-down assays were unsuccessful (data not shown), but we were able to show that the AMIN domain directly interacts with the peptidoglycan. Because the AMIN domain is known to be sufficient for the localization of AmiC at the division site, it likely recognizes a specific characteristic of the septal peptidoglycan which remains, however, to be identified. Therefore, the AMIN domain seems to play the role of a septal peptidoglycan anchor that helps to localize the amidase_3 domain to the division site. The amidase activity of AmiC is thus spatially targeted by the AMIN domain and activated by the LytM domain of NlpD which also localizes to the division site.

AmiB is known to be targeted to the cell division site via its N-terminal region (Peters *et al*., 2011). Secondary structure prediction attributes eight β-strands to this N-terminal targeting domain. However, sequence alignment with the AMIN domain of AmiC (25.8% identity) shows strong similarities only with the conserved amino-acids of the β-sheet2: four identical and three equivalent out of nine residues. For the β-sheet1, only one residue is strictly conserved and one is equivalent. Therefore, unlike the large majority of protein sharing the AMIN-amidase_3 architecture of AmiC, AmiB is characterized by relatively conserved residues on the β-sheet2 but lacks the conserved ones highlighted on the β-sheet1 of AmiC. To our knowledge, AmiB is not in any way deficient in localization at the septum compared with AmiC. The advantage of a symmetrical AMIN domain shared by most homologues of AmiC remains therefore unclear.

Conclusions

The AmiC structure highlights the importance of a helix obstructing the active site of this enzyme. We have shown that an AmiC variant lacking this helix is constitutively active and that the addition of a synthetic α5 helix peptide restores the inhibited form of the enzyme. Together with the direct interaction between AmiC and NlpD *in vitro*, these results strongly suggest that the displacement of this helix by the cognate AmiC activator NlpD is the basis of the AmiC activation as proposed by Yang *et al*. (2012). The linker connecting the AMIN domain to the catalytic domain could facilitate the activation by NlpD and regulate its spatial localization between the outer membrane and the newly synthesized peptidoglycan layer. Finally, the peptidoglycan binding capacity of the AMIN domain along with its requirement for a proper localization of AmiC at the division site (Bernhardt and de Boer, 2003) argues for a specific recog-

nition of the septal peptidoglycan in order to properly position AmiC at the septum.

Experimental procedures

Cloning, overexpression and purification

Escherichia coli K12 genomic DNA was used for PCR amplification of *amiC* and *nlpD* genes with the following primers: 5′-GCGCATATGGGGCGCGATCGTCCGATTG-3′; 5′-CGCTCGAGTCATCCCCTTCTCGCCAGC-3′ for *amiC* and 5′-GCGCATATGTCTGACACTTCAAATCCACCGGCACC-3′; 5′-CGCTCGAGTTATCGCTGCGGCAAATAACGCAG-3′ for *nlpD*. For AmiC, the amplified gene codes for a protein without its signal peptide (Gln35-Gly417). NlpD is also produced without its signal peptide (Ser27-Arg380). The gene coding for the AMIN domain (Gln35-Ala145) was amplified with the following primers: 5′-GCGCATATGCAGGTCGTGGCGGTGCGC-3′; 5′-CGCTCGAGTTAGGCCGGATAGAGGTCCATCACC-3′. PCR products have been cloned into pET28-MHL vector (SGC consortium) between NdeI and XhoI sites allowing the expression of the proteins with a 6xHis Tag followed by a TEV cleavage site at the N-terminal position. The gene coding for AmiC lacking residues Ala287 to Ile329 (called AmiCΔH5) was synthesized *de novo* (Geneart GmbH, Regensburg, Germany) and cloned into pET28-MHL between NdeI and XhoI. After cleavage of the 6xHis Tag with the TEV protease, all the proteins produced with the pET28-MHL contain three additional N-terminal amino acids (Gly-His-Met).

Transformed C43 (DE3) cells were grown in TB medium supplemented with kanamycin (50 μg ml^{-1}) until the OD_{600} reached 0.8. The culture was then induced with 0.5 mM IPTG for 3 h at 28°C. The cells were harvested by centrifugation (4000 *g*, 20 min, 4°C) and the pellet was resuspended in the lysis buffer (30 mM Tris/HCl pH 7.5, 300 mM NaCl, 10% Glycerol, 2 mM MgSO4, 1.5 U ml^{-1} benzonase) before disruption using an Emulsiflex C3 homogenizer. The lysate was spun down at 40 000 *g* for 30 min and the supernatant was filtered through a 0.22 μm membrane (Millex-GP, Millipore) before purification.

The sample was loaded onto a HisTrap column (GE Healthcare) equilibrated with buffer A (30 mM Tris-HCl pH 7.5, 300 mM NaCl, 10% Glycerol). The column was washed with Buffer A containing 50 mM Imidazole and the proteins were eluted with increasing concentration of imidazole in buffer A: between 50 and 100 mM for NlpD and between 150 and 200 mM for AmiC and the AMIN domain. AmiCΔH5 was isolated by batch purification with Ni-NTA agarose gel (GE Healthcare) and eluted at 250–300 mM imidazole in buffer A. After SDS-PAGE analysis pure fractions were pooled and dialysed overnight against buffer A, frozen with liquid nitrogen and stored at −80°C at approximately 30 μM. For interaction and activity tests, His-tags were removed by an overnight incubation at 4°C with the TEV-protease. The cleaved tags, the uncleaved protein and the His-tagged TEV-protease were removed by a second passage on a HisTrap column (GE Healthcare).

Crystallization and data collection

His-tagged AmiC was concentrated to 13 mg ml^{-1} and crystallized using the hanging-drop vapour diffusion method. 1 μl of protein was mixed with 1 μl of precipitant buffer (20% PEG 8000, 0.1 M CABS pH 12, 20 mM $CoCl_2$) and crystals grew at room temperature. The crystals were transferred into a cryoprotectant solution containing 50% glycerol before flash-freezing in a liquid nitrogen bath. Diffraction data were collected at the European Synchrotron Radiation Source Facility FIP-BM30a beamline (Grenoble).

Data processing

Data were integrated and scaled with Mosflm (Leslie and Powell, 2007) and Scala from the CCP4 software package (1994). A first model of the catalytic domain of AmiC was determined by molecular replacement using the structure of AmiB from *B. henselae* as a search model (PDB ID: 3ne8). Five poly-alanine β-strands of the N-terminal AMIN domain were built in the electron density and subjected to a DALI search. The most structurally related structure, the chaperone Hsp26, was used as a template to build seven poly-alanine β-strands of the AMIN domain. This partial model was provided to the software ARP/wARP (Morris *et al*., 2003) to build and assign the whole domain. Helix α2 was solved by fitting the Leu140-Leu144 (LLALL) segment in the electron density and, although the density was less clear for the residues, the helix could be completed from Pro139 to Asn148.

Structure analysis

The ConSurf server was used to analyse the amino acid conservation on the surface of AmiC (http://consurf.tau.ac.il/) (Ashkenazy *et al*., 2010). The homologous sequences were selected using three iterations of CSI-Blast within the UNIREF-90 database and the 150 most representative sequences were used to generate conservation scores (Table S1). The PISA server provided an analysis of the interface between N and C-terminal domains (http://www.ebi.ac.uk/msd-srv/prot_int/pistart.html) (Krissinel and Henrick, 2007). The different figures were generated with Chimera (Pettersen *et al*., 2004).

Preparation of peptidoglycan sacculi and labelling with Remazol Brilliant Blue

Peptidoglycan sacculi were prepared from MC1061 cells as described earlier (Glauner *et al*., 1988). The RBB-labelled peptidoglycan was prepared as described (Uehara *et al*., 2009). The sacculi were incubated overnight with 20 mM RBB (Sigma) in 0.25 M NaOH at 37°C. The next morning, the sample was neutralized by addition of HCl before centrifugation (16 000 *g*, 20 min, room temperature). The pelleted sacculi were then washed with MilliQ water until no more soluble RBB was detected after centrifugation. The labelled sacculi were finally resuspended in water with 0.02% sodium azide and stored at 4°C.

Activity tests with RBB-labelled peptidoglycan

For activity tests, 10 μl of the RBB-PG were incubated with 4 μM of AmiC and/or NlpD (without His tag) in 30 mM Tris/HCl buffer pH 7.5, 300 mM NaCl and 10% glycerol (100 μl total) for 30 min to 15 h (overnight) in a total volume of 100 μl. The

samples were centrifuged for 10 min at 14 000 *g* and the absorbance of the supernatant was measured at 595 nm (Tecan Infinite 200 PRO microplate reader, Tecan Austria GmbH, Austria). Reported results were standardized with a negative control consisting of 10 µl of RBB-PG and 90 µl of the aforementioned buffer. Lysozyme was used as a positive control at a 4 µM concentration. The peptide corresponding to the α5 helix (Thr288-Gly306) was synthesized by Genscript (NJ, USA).

Peptidoglycan-binding assay

The pull down experiments were carried out with the untagged AMIN domain. 10 µg of protein was incubated 2 h either with or without peptidoglycan in the binding buffer (30 mM Tris pH 6.8, 50 mM NaCl, 10 mM $MgCl_2$) in a total volume of 100 µl. The samples were centrifuged for 20 min at 14 000 *g*. The pellets were washed twice in 150 µl of binding buffer and then resuspended in 40 µl of SDS 2% and incubated for 1 h. The supernatants of the binding step, the washing steps and the resuspended pellet were analysed by SDS-PAGE.

Microscale thermophoresis

Interactions between freshly prepared AmiC and NlpD (without 6x His Tags) were measured using microscale thermophoresis (Jerabek-Willemsen *et al*., 2011) with a Monolith NT.115 (NanoTemper Technologies GmbH, Munich, Germany). Each protein was in turn labelled with DyLight 650 (Thermo Scientific) and mixed with sixteen twofold serial dilutions of the other unlabelled protein starting from 272 µM for AmiC and 426 µM for NlpD. The final buffer contained 50 mM Tris-HCl pH 7.5, 150 mM NaCl, 10 mM MgCl2, 0.05 % Tween-20 and measurement were performed in hydrophilic capillaries with 100% Led power and 80% IR-laser power. NanoTemper Analysis 1.2.101 software was used for the fitting of the data and determination of the apparent Kd values. The experiments were preformed three times for each combination.

Accession code

Atomic coordinates and experimental structure factors for AmiC have been deposited in the Protein Data Bank under the accession code 4BIN.

Acknowledgements

We thank Jean-Marie Frère for critical reading of the manuscript. We also thank the staff of beamline BM30a at ESRF for assistance in X-ray data collection. This work was supported in part by the European Commission Sixth Framework Program grants LSMH-CT-EUR-INTAFAR 2004-512138, by the Belgian Program on Interuniversity Poles of Attraction initiated by the Belgian State, Prime Minister's Office, Science Policy programming (IAP no. P6/19 and P7/44), by the Fonds de la Recherche Scientifique (IISN 4.4509.09, IISN 4.4503.11) and the University of Liège (Fonds spéciaux, Crédit classique). M. R. is recipient of a FRIA (Fonds de la Recherche pour l'Industrie et l'Agriculture) fellowship (F.R.S.-FNRS, Brussels, Belgium). F. K. and M. T. are research associates of the FRS-FNRS.

References

Ashkenazy, H., Erez, E., Martz, E., Pupko, T., and Ben-Tal, N. (2010) ConSurf 2010: calculating evolutionary conservation in sequence and structure of proteins and nucleic acids. *Nucleic Acids Res* **38:** W529–W533.

Bernhardt, T.G., and De Boer, P.A.J. (2003) The *Escherichia coli* amidase AmiC is a periplasmic septal ring component exported via the twin-arginine transport pathway. *Mol Microbiol* **48:** 1171–1182.

Bertsche, U., Kast, T., Wolf, B., Fraipont, C., Aarsman, M.E.G., Kannenberg, K., *et al*. (2006) Interaction between two murein (peptidoglycan) synthases, PBP3 and PBP1B, in *Escherichia coli*. *Mol Microbiol* **61:** 675–690.

Bi, E.F., and Lutkenhaus, J. (1991) FtsZ ring structure associated with division in *Escherichia coli*. *Nature* **354:** 161–164.

Botta, G.A., and Park, J.T. (1981) Evidence for involvement of penicillin-binding protein 3 in murein synthesis during septation but not during cell elongation. *J Bacteriol* **145:** 333–340.

Buddelmeijer, N., and Beckwith, J. (2004) A complex of the *Escherichia coli* cell division proteins FtsL, FtsB and FtsQ forms independently of its localization to the septal region. *Mol Microbiol* **52:** 1315–1327.

Christianson, D.W., Mangani, S., Shoham, G., and Lipscomb, W.N. (1989) Binding of D-phenylalanine and D-tyrosine to carboxypeptidase A. *J Biol Chem* **264:** 12849–12853.

Collier, J. (2010) A new factor stimulating peptidoglycan hydrolysis to separate daughter cells in *Caulobacter crescentus*. *Mol Microbiol* **77:** 11–14.

Corbin, B.D., Wang, Y., Beuria, T.K., and Margolin, W. (2007) Interaction between cell division proteins FtsE and FtsZ. *J Bacteriol* **189:** 3026–3035.

De Souza, R.F., Anantharaman, V., De Souza, S.J., Aravind, L., and Gueiros-Filho, F.J. (2008) AMIN domains have a predicted role in localization of diverse periplasmic protein complexes. *Bioinformatics* **24:** 2423–2426.

Den Blaauwen, T., De Pedro, M.A., Nguyen-Distèche, M., and Ayala, J.A. (2008) Morphogenesis of rod-shaped sacculi. *FEMS Microbiol Rev* **32:** 321–344.

Durand-Heredia, J., Rivkin, E., Fan, G., Morales, J., and Janakiraman, A. (2012) Identification of ZapD as a cell division factor that promotes the assembly of FtsZ in *Escherichia coli*. *J Bacteriol* **194:** 3189–3198.

Durand-Heredia, J.M., Yu, H.H., De Carlo, S., Lesser, C.F., and Janakiraman, A. (2011) Identification and characterization of ZapC, a stabilizer of the FtsZ ring in *Escherichia coli*. *J Bacteriol* **193:** 1405–1413.

Fraipont, C., Alexeeva, S., Wolf, B., Van Der Ploeg, R., Schloesser, M., Den Blaauwen, T., and Nguyen-Distèche, M. (2011) The integral membrane FtsW protein and peptidoglycan synthase PBP3 form a subcomplex in *Escherichia coli*. *Microbiology* **157:** 251–259.

Galli, E., and Gerdes, K. (2012) FtsZ-ZapA-ZapB interactome of *Escherichia coli*. *J Bacteriol* **194:** 292–302.

Glauner, B., Höltje, J.V., and Schwarz, U. (1988) The composition of the murein of *Escherichia coli*. *J Biol Chem* **263:** 10088–10095.

Goehring, N.W., Gonzalez, M.D., and Beckwith, J. (2006) Premature targeting of cell division proteins to midcell reveals hierarchies of protein interactions involved in divisome assembly. *Mol Microbiol* **61:** 33–45.

Hale, C.A., and De Boer, P.A.J. (1997) Direct binding of FtsZ to ZipA, an essential component of the septal ring structure that mediates cell division in *E. coli*. *Cell* **88:** 175–185.

Heidrich, C., Templin, M.F., Ursinus, A., Merdanovic, M., Berger, J., Schwarz, H., *et al.* (2001) Involvement of N-acetylmuramyl-L-alanine amidases in cell separation and antibiotic-induced autolysis of *Escherichia coli*. *Mol Microbiol* **41:** 167–178.

Jerabek-Willemsen, M., Wienken, C.J., Braun, D., Baaske, P., and Duhr, S. (2011) Molecular interaction studies using microscale thermophoresis. *Assay Drug Dev Technol* **9:** 342–353.

Korndörfer, I.P., Danzer, J., Schmelcher, M., Zimmer, M., Skerra, A., and Loessner, M.J. (2006) The crystal structure of the bacteriophage PSA endolysin reveals a unique fold responsible for specific recognition of Listeria cell walls. *J Mol Biol* **364:** 678–689.

Krissinel, E., and Henrick, K. (2007) Inference of macromolecular assemblies from crystalline state. *J Mol Biol* **372:** 774–797.

Leslie, A.G.W., and Powell, H.R. (2007) Processing diffraction data with mosflm. In *Evolving Methods for Macromolecular Crystallography*. Read, R.J., and Sussman, J.L. (eds). Dordrecht: Springer Netherlands, pp. 41–51.

Mayer, M.J., Garefalaki, V., Spoerl, R., Narbad, A., and Meijers, R. (2011) Structure-based modification of a *Clostridium difficile*-targeting endolysin affects activity and host range. *J Bacteriol* **193:** 5477–5486.

Möll, A., Schlimpert, S., Briegel, A., Jensen, G.J., and Thanbichler, M. (2010) DipM, a new factor required for peptidoglycan remodelling during cell division in *Caulobacter crescentus*. *Mol Microbiol* **77:** 90–107.

Morris, R.J., Perrakis, A., and Lamzin, V.S. (2003) ARP/wARP and automatic interpretation of protein electron density maps. *Methods Enzymol* **374:** 229–244.

Müller, P., Ewers, C., Bertsche, U., Anstett, M., Kallis, T., Breukink, E., *et al.* (2007) The essential cell division protein FtsN interacts with the murein (peptidoglycan) synthase PBP1B in *Escherichia coli*. *J Biol Chem* **282:** 36394–36402.

Paradis-Bleau, C., Markovski, M., Uehara, T., Lupoli, T.J., Walker, S., Kahne, D.E., and Bernhardt, T.G. (2010) Lipoprotein cofactors located in the outer membrane activate bacterial cell wall polymerases. *Cell* **143:** 1110–1120.

Peters, N.T., Dinh, T., and Bernhardt, T.G. (2011) A fail-safe mechanism in the septal ring assembly pathway generated by the sequential recruitment of cell separation amidases and their activators. *J Bacteriol* **193:** 4973–4983.

Peters, N.T., Morlot, C., Yang, D.C., Uehara, T., Vernet, T., and Bernhardt, T.G. (2013) Structure-function analysis of the LytM domain of EnvC, an activator of cell wall remodelling at the *Escherichia coli* division site. *Mol Microbiol* **89:** 690–701.

Pettersen, E.F., Goddard, T.D., Huang, C.C., Couch, G.S., Greenblatt, D.M., Meng, E.C., and Ferrin, T.E. (2004) UCSF Chimera – a visualization system for exploratory research and analysis. *J Comput Chem* **25:** 1605–1612.

Poggio, S., Takacs, C.N., Vollmer, W., and Jacobs-Wagner, C. (2010) A protein critical for cell constriction in the Gram-negative bacterium *Caulobacter crescentus* localizes at the division site through its peptidoglycan-binding LysM domains. *Mol Microbiol* **77:** 74–89.

Spratt, B.G. (1975) Distinct penicillin binding proteins involved in the division, elongation, and shape of *Escherichia coli* K12. *Proc Natl Acad Sci USA* **72:** 2999–3003.

Sycuro, L.K., Pincus, Z., Gutierrez, K.D., Biboy, J., Stern, C.A., Vollmer, W., and Salama, N.R. (2010) Peptidoglycan crosslinking relaxation promotes *Helicobacter pylori*'s helical shape and stomach colonization. *Cell* **141:** 822–833.

Typas, A., Banzhaf, M., Van Den Berg Van Saparoea, B., Verheul, J., Biboy, J., Nichols, R.J., *et al.* (2010) Regulation of peptidoglycan synthesis by outer-membrane proteins. *Cell* **143:** 1097–1109.

Uehara, T., Dinh, T., and Bernhardt, T.G. (2009) LytM-domain factors are required for daughter cell separation and rapid ampicillin-induced lysis in *Escherichia coli*. *J Bacteriol* **191:** 5094–5107.

Uehara, T., Parzych, K.R., Dinh, T., and Bernhardt, T.G. (2010) Daughter cell separation is controlled by cytokinetic ring-activated cell wall hydrolysis. *EMBO J* **29:** 1412–1422.

Weiss, M.S., and Hilgenfeld, R. (1997) On the use of the merging R factor as a quality indicator for X-ray data. *J Appl Crystallogr* **30:** 203–205.

Yang, D.C., Peters, N.T., Parzych, K.R., Uehara, T., Markovski, M., and Bernhardt, T.G. (2011) An ATP-binding cassette transporter-like complex governs cell-wall hydrolysis at the bacterial cytokinetic ring. *Proc Natl Acad Sci USA* **108:** 18209–18210.

Yang, D.C., Tan, K., Joachimiak, A., and Bernhardt, T.G. (2012) A conformational switch controls cell wall-remodelling enzymes required for bacterial cell division. *Mol Microbiol* **85:** 768–781.

Supporting information

Additional supporting information may be found in the online version of this article at the publisher's web-site.